Materials Research Bulletin 46 (2011) 1219–1226

Contents lists available at ScienceDirect

Materials Research Bulletin

journal homepage: www.elsevier.com/locate/matresbu

Preparation and characterization of rare earth orthoborates, $LnBO_3$ (Ln = Tb, La, Pr, Nd, Sm, Eu, Gd, Dy, Y) and $LaBO_3$:Gd, Tb, Eu by metathesis reaction: ESR of $LaBO_3$:Gd and luminescence of $LaBO_3$:Tb, Eu

Radha Velchuri [a], B. Vijaya Kumar [a], V. Rama Devi [a], G. Prasad [b], D. Jaya Prakash [c], M. Vithal [a,*]

[a] Department of Chemistry, Osmania University, Hyderabad 500007, India
[b] Department of Physics, Osmania University, Hyderabad 500007, India
[c] College of Technology, Osmania University, Hyderabad 500007, India

ARTICLE INFO

Article history:
Received 6 October 2010
Received in revised form 29 March 2011
Accepted 11 April 2011
Available online 19 April 2011

Keywords:
C. Infrared spectroscopy
C. X-ray diffraction
D. Electron paramagnetic resonance
D. Luminescence
D. Optical properties

ABSTRACT

Lanthanide orthoborates of composition $LnBO_3$ (Ln = Tb, La, Pr, Nd, Sm, Eu, Gd, Dy, Y) and $LaBO_3$:Gd, Tb, Eu have been prepared by metathesis reaction. This method provides a convenient route for the synthesis of orthoborates and its solid solutions at low temperatures. Powder X-ray diffraction and FT-IR spectroscopy were used to characterize these borates. Rare earth borates, ($LnBO_3$) are isomorphous with different forms of $CaCO_3$ depending on the radius of rare earth ion. $LaBO_3$, $LaBO_3$:Gd, Tb, Eu, $PrBO_3$, $NdBO_3$ crystallized in aragonite structure, $SmBO_3$ crystallized in H-form and $TbBO_3$, $EuBO_3$, $GdBO_3$, $DyBO_3$, YBO_3 crystallized in vaterite structure. The structural analysis of $TbBO_3$ was carried out. The morphology of these borates was obtained from Scanning electron microscopy. Spin-Hamiltonian parameters for Gd^{3+} are deduced from room temperature electron spin resonance spectrum of $LaBO_3$:Gd. The luminescence of $LaBO_3$:Tb, Eu gave characteristics peaks corresponding to Tb^{3+}, Eu^{3+} respectively.

1. Introduction

Transition metal and rare earth orthoborates of composition $LnBO_3$ (Ln = trivalent transition or rare earth ion) have attracted considerable attention owing to their remarkable properties and potential applications. For instance ferric borate, $FeBO_3$, is a canted antiferromagnet with calcite structure and has favorable magnetic properties for high-speed magneto-optical applications [1,2]. Calcite type VBO_3 and $CrBO_3$ also possess interesting magnetic properties [3]. Rare earth orthoborates of composition $LnBO_3$ (Ln = Gd, Y, etc.), on the other hand, are found to be promising host materials for VUV phosphors [4]. High VUV transparency and exceptional optical damage threshold of $LnBO_3$ type materials makes them worthy of investigations. Keszler has reviewed the potential applications of transition metal and rare earth borates [5]. It is well known that phosphors based on orthoborates have attracted much attention due to their high stability and low synthetic temperature. Rare earth doped orthoborates are good host lattices for luminescence of Eu^{3+}, Tb^{3+} and used in flat displays, mercury-free fluorescent tubes etc. For example, (Y, Gd)BO_3:Eu^{3+}/Tb^{3+} has found application in plasma display panels (PDPs) as a red/green phosphor [6–9].

Rare earth orthoborates, $LnBO_3$, are isomorphous with $CaCO_3$. These rare earth borates crystallize in aragonite, vaterite and calcite forms similar to that of $CaCO_3$. It is observed that the type of crystal lattice adopted by the lanthanide borate depends on the radius ratio of Ln^{3+} and O^{2-} (Ln^{3+}/O^{2-}). Lanthanide borates having a radius ratio (Ln^{3+}/O^{2-}) of 0.71 and above crystallize in aragonite structure (e.g. $LaBO_3$, $NdBO_3$). If the radius ratio is in the range 0.71–0.61, the corresponding borate crystallizes in vaterite structure ($SmBO_3$–$YbBO_3$). Borates having the radius ratio 0.607 and less adopt both calcite and vaterite structures depending on the preparation temperature [10]. Aragonite structure is characterized by a nine coordinated central metal ion (Ln^{3+}) in a hexagonal close packing of orthorhombic unit cell with *Pnam*(62) space group [11]. Vaterite type $LnBO_3$ materials crystallize in hexagonal lattice with $P6_3/m$(176) space group and the lanthanide ion is coordinated to eight oxygen atoms in a trigonal bicapped antiprism [12]. The calcite structure has rhombohedral symmetry with space group $R\bar{3}C$ (Z = 6) and the lanthanide ion is in six coordination [13]. In addition to these three forms, some of these rare earth orthoborates also exist in 'high temperature form' (H-form) which is quite different from these structures.

The properties of the materials depend on the method of preparation, sample purity and particle distribution [14]. It is observed that use of alternative synthesis routes such as wet process [15], flux evaporation [12], ball milling [16], hydrothermal [17,18] and metathesis method offer the possibility of obtaining

* Corresponding author. Tel.: +91 40 276823237; fax: +91 40 27090020.
E-mail address: muga_vithal@rediffmail.com (M. Vithal).

0025-5408/$ – see front matter © 2011 Elsevier Ltd. All rights reserved.
doi:10.1016/j.materresbull.2011.04.006

high purity materials and some times the micro structure/morphology control. To our knowledge, this is the first attempt to prepare lanthanide orthoborates $LnBO_3$ and its solid solutions by metathesis approach at temperatures which are lower than reported [7,10,12,16,19–21]. In this paper, we present the preparation of orthoborates $LnBO_3$ (Ln = Tb, La, Pr, Nd, Sm, Eu, Gd, Dy, Y) and $LaBO_3$:Gd, Tb, Eu by metathesis approach employing $LnCl_3$ and $NaBO_2$. ESR of $LaBO_3$:Gd and luminescence of $LaBO_3$:Tb, Eu is also presented.

2. Experimental

2.1. Metathesis synthesis

Stoichiometric amounts of Tb_4O_7 or Ln_2O_3 (Ln = La, Nd, Sm, Eu, Gd, Dy, Y) or Pr_6O_{11} required for $LnBO_3$ (Ln = Tb, La, Pr, Nd, Sm, Eu, Gd, Dy, Y) and $LaBO_3$:Gd, Tb, Eu (2.5, 5, 7.5 and 10 mol%) compositions are dissolved in concentrated HCl to obtain aqueous $LnCl_3$ solutions. This solution is evaporated to dryness to expel excess HCl. The dried $LnCl_3$ solid and 10% excess $NaBO_2$ are ground thoroughly using spectral grade acetone. All the resultant materials are heated at 650 °C/14 h except $LaBO_3$, $NdBO_3$, $SmBO_3$, $EuBO_3$ and $GdBO_3$, which are sintered at both 650 and 900 °C/6 h. The obtained products are washed with de-ionized hot water several times to remove NaCl, B_2O_3 and $NaBO_2$. The remaining solid is dried on a hot plate. The probable reactions for orthoborates and their solid solutions are given below.

$$LnCl_3 + 3NaBO_2 \xrightarrow{650\,^\circ C/14\,h} LnBO_3 + B_2O_3 + 3NaCl \quad (1)$$

$$(1-x)LaCl_3 + xLnCl_3 + 3NaBO_2 \xrightarrow{650\,^\circ C/14\,h} La_{1-x}Ln_xBO_3 + B_2O_3 + 3NaCl$$
$$(Ln = Gd, Tb \text{ and } Eu;\ x = 0.025, 0.05, 0.075 \text{ and } 0.1) \quad (2)$$

2.2. Solid state method

Stoichiometric amounts of H_3BO_3 and Tb_4O_7 or Ln_2O_3 (Ln = La, Nd, Sm, Eu, Gd, Dy, Y) or Pr_6O_{11} required for $LnBO_3$ (Ln = Tb, La, Pr, Nd, Sm, Eu, Gd, Dy, Y) composition are ground thoroughly using spectral grade acetone for several hours. The resultant materials are heated at 500 °C/5 h, 700 °C/5 h, and 900 °C/5 h with intermediate grindings.

The powder X-ray diffractograms are recorded at room temperature on Shimadzu XRD-7000 powder X-ray diffractometer using Ni filtered monochromatic Cu-Kα radiation of wavelength 1.5406 Å. The scan speed is 2°/min in the range 2θ = 10–80°. Infrared spectra were recorded in the form of KBr pellets in the wave number range 1500–400 cm^{-1} using JASCO IR-5300 spectrometer. SEM images were recorded on the HITACHI S-3700N variable pressure scanning electron microscope (VP-SEM). Room temperature ESR spectra were recorded on a JOEL PE-3X, X-band spectrometer equipped with a 100 kHz field modulation unit. The ESR spectrometer was optimized for modulation amplitude receiver gain, time constant and scans time. The luminescence spectra are recorded with Fluorolog spectrophotometer equipped with a 40 W Xenon lamp as the excitation source of radiation at room temperature. Cylindrical pellets (≈10 mm diameter and ≈3 mm thickness) of the samples are obtained by applying uniaxial pressure of 200 MPa. The pellets are sintered at 900 °C for 4 h (for density measurements) and coated with silver paint (for AC conductivity measurements). Experimental densities of sintered pellets are measured by Archimedes principle using xylene as immersion liquid. Theoretical (from X-ray diffraction) densities are obtained from unit cell dimensions. AC Impedance and conductivity measurements are carried out using HP4192A Impedance analyzer at room temperature in the frequency range 100 Hz–1 MHz.

3. Results and discussion

3.1. Powder XRD

The powder XRD patterns of the product obtained by the reaction between $NaBO_2$ and $TbCl_3$ (at 650 °C) before and after washing with de-ionized water are shown in Fig. 1(a) and (b) respectively. The powder XRD of sample before washing was characterized by peaks belonging to $TbBO_3$, NaCl (marked as *), $NaBO_2$ (represented as △), B_2O_3 (shown as □) and $TbCl_3$ phases (represented as #) (Fig. 1(a)). The presence of diffraction peaks corresponding to $TbBO_3$, NaCl and B_2O_3 indicate that the reaction has taken place in a metathetic pathway as shown in equation 1. The excess $NaBO_2$ and unreacted $TbCl_3$ also appear as weak diffraction lines. Fig. 1(b) shows the powder XRD pattern of the product obtained after washing with de-ionized water. All the observed d-lines are consistent with reported $TbBO_3$ [JCPDS No. 24-1272] and free from impurities. The structural analysis of $TbBO_3$ is carried by Rietveld refinement program MAUD. It crystallizes in hexagonal lattice (vaterite structure) with space group $P6_3/m$. The observed and calculated XRD patterns are shown in Fig. 2. The reliability factors obtained from the refinement are R_{wp} = 21.7%, R_p = 15.2%, R_{exp} = 16.49%. The unit cell parameters obtained for a and c are 3.813 ± 0.02 and 8.879 ± 0.02 Å respectively, which are close to the reported values [JCPDS Card No. 24-1272]. The atomic coordinates of $TbBO_3$ obtained from the Rietveld analysis are given in Table 1.

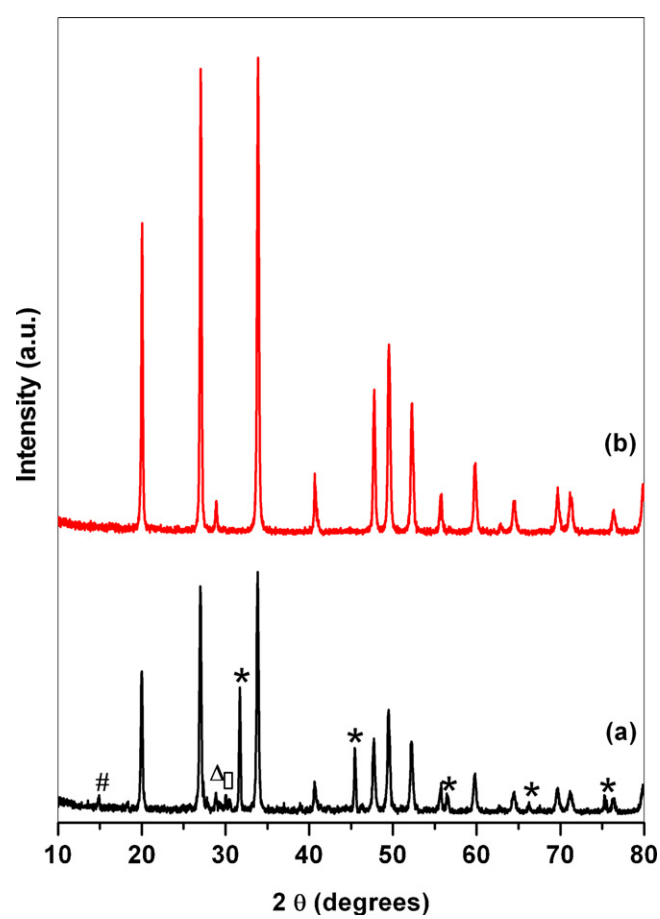

Fig. 1. Powder XRD patterns of $TbBO_3$ prepared at 650 °C (a) before washing and (b) after washing with de-ionized water.

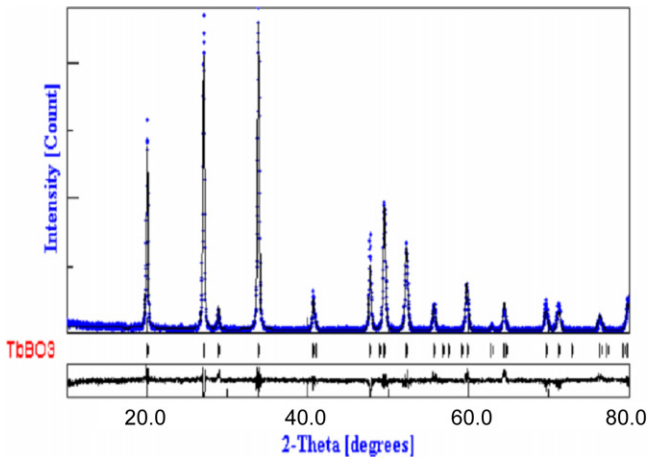

Fig. 2. Observed and calculated XRD patterns of $TbBO_3$.

Table 1
Atomic coordinates of $TbBO_3$.

Element	Wyckoff position	Site occupancy	*x*	*y*	*z*
Tb	2b	1	0	0	0
O(1)	4f	1	0.667	0.333	0.108
O(2)	6h	1/3	0.770	−0.159	0.25
B	6h	1/3	0.642	0.489	0.25

The powder XRD patterns of $LaBO_3$:Gd, Tb, Eu after washing with de-ionized water are found to be similar with each other and comparable with reported data for $LaBO_3$ [JCPDS No. 12-0762]. Fig. 3(a)–(e) shows the powder XRD patterns of $LaBO_3$:Gd (0, 2.5, 5, 7.5 and 10 mol%). These patterns (prepared at 650 °C) have d-lines belonging to only aragonite structure without any trace of H-$LaBO_3$ impurities. Further, it was also noticed that no H-$LaBO_3$ was formed when the sample was prepared at 900 °C. The X-ray powder patterns of $LaBO_3$:Gd, Tb, Eu were analyzed using least square fit method employing the POWD software [22] to obtain the unit cell parameters. The observed d-lines and unit cell parameters of $LaBO_3$ were given as input parameters to obtain the calculated d-lines and unit cell parameters. $LaBO_3$:Gd, Tb, Eu samples were found to crystallize in orthorhombic lattice (aragonite structure) with *Pnam*(62) space group. It is noticed that for low concentrations of dopant ion (≤ 10 mol%), single phase materials were obtained. When the concentrations of dopant are above 10 mol%, a mixture of phases was obtained. Thus, the metathesis reactions in the present investigation are useful for the preparation of solid solutions when the dopant concentration is low.

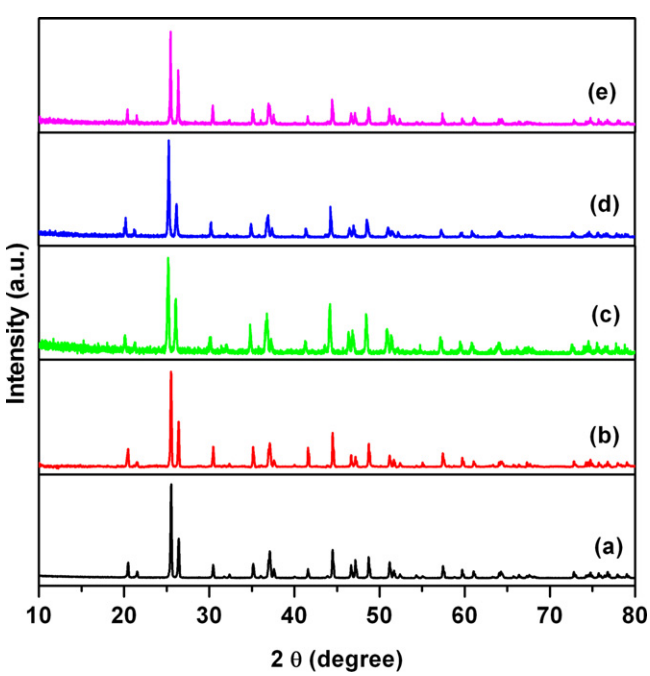

Fig. 3. Powder XRD patterns of $LaBO_3$:Gd (a) 0 mol%, (b) 2.5 mol%, (c) 5 mol%, (d) 7.5 mol% and (e) 10 mol% prepared at 650 °C.

The powder XRD of $PrBO_3$ prepared at 650 °C is shown in Fig. 4(a). The d-lines $PrBO_3$ are similar to the d-lines of $LaBO_3$ and $NdBO_3$. Since the ionic radii of Pr^{3+} (1.06), La^{3+} (1.14) and Nd^{3+} (1.04) are approximately same and the fact that the ratio of Ln^{3+}/O^{2-} (Ln = Pr, La and Nd) falls in the range 0.81–0.74, they are expected to crystallize in aragonite structure [10]. To our knowledge, the d-lines of $PrBO_3$ are not indexed. However, Tananaev has reported the observed d-lines for $PrBO_3$ ([23], JCPDS No. 23-1384) and Laureiro et al. have reported the lattice parameters of $PrBO_3$ and noticed that both $PrBO_3$ and $NdBO_3$ are isomorphous [24]. Therefore, the d-lines of $PrBO_3$ are least square fitted and the unit cell parameters of $NdBO_3$ are given as input parameters. The unit cell parameters of $PrBO_3$ were found to be a = 5.74, b = 8.09, c = 5.05 Å. These unit cell parameters are close to those reported [24]. It crystallizes in orthorhombic lattice with aragonite structure and the space group is *Pnam*(62).

Fig. 4(b) and (c) shows the powder XRD patterns of $NdBO_3$ prepared at 900 and 650 °C respectively. The d-lines of the product obtained at 650 °C are consistent with reported d-lines [JCPDS No 12-0756] corresponding to orthorhombic lattice with aragonite structure. However, some additional lines (shown by * in Fig. 4(c))

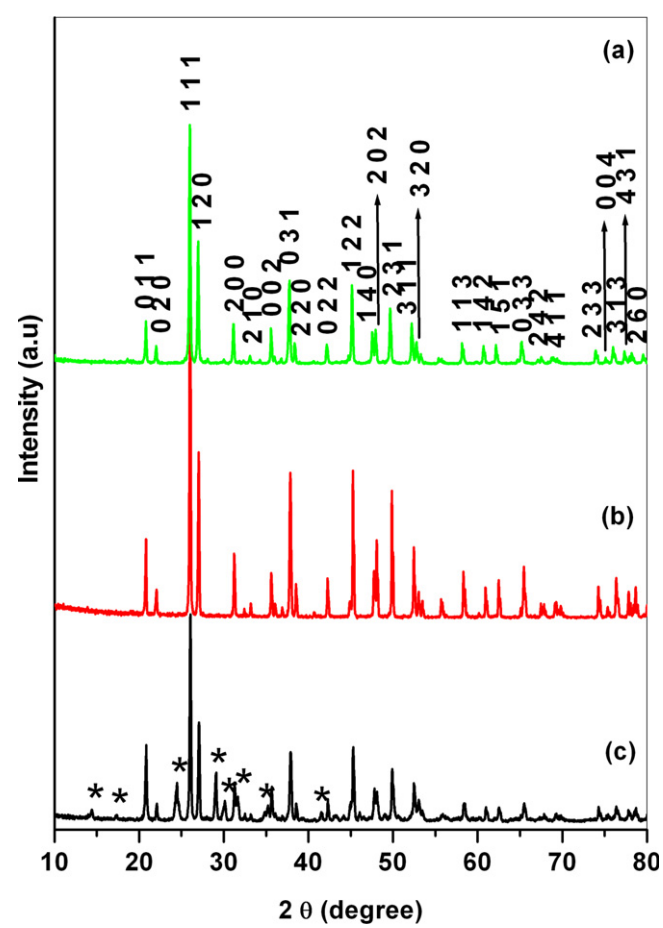

Fig. 4. Powder XRD patterns of (a) $PrBO_3$ prepared at 650 °C, (b) $NdBO_3$ prepared at 900 °C and (c) 650 °C.

of low intensity belonging to high temperature form, H-$NdBO_3$, were also observed [JCPDS No 13-0488]. Additional experiments were carried out to obtain phase pure $NdBO_3$ (aragonite). The sample prepared at 900 °C shows only d-lines belonging to $NdBO_3$ (aragonite) without any trace of H-$NdBO_3$ (Fig. 4(b)). This is consistent with the results reported earlier [15].

The powder XRD pattern of $SmBO_3$ prepared at 650 °C consists of d-lines corresponding to H-$SmBO_3$ [JCPDS No. 13-0489] (major) and vaterite $SmBO_3$ [JCPDS No. 74-1930] (minor). $SmBO_3$ is known to exhibit phase transformations from H-$SmBO_3$ to $SmBO_3$ (vaterite) at 1100 °C and back to H-form at 1300 °C when prepared by wet process [15]. It was also reported that H-$SmBO_3$ is never obtained in pure form at low temperature. The sample prepared at 900 °C is characterized by d-lines belonging to only H-form. Thus, our observations are consistent with earlier reported results [15].

Fig. 5(a) and (c) shows the powder XRD patterns of $EuBO_3$ and $GdBO_3$ prepared at 650 °C. Both the patterns were characterized by d-lines belonging to hexagonal vaterite and a few less intense lines (indicated by * in Fig. 5(a) and (c)), possibly belonging to H-forms of $EuBO_3$ and $GdBO_3$. All the d-lines (except indicated by *) are consistent with the reported JCPDS data [JCPDS Nos. 74-1931 for $EuBO_3$ and 74-1932 for $GdBO_3$]. The d-lines corresponding to H-$EuBO_3$ are similar to those reported by Lemanaue et al. [15]. The positions (2θ) of less intense d-lines (indicated by *) observed in $GdBO_3$ are similar to the d-lines observed in H-$EuBO_3$ and therefore may be due to high temperature form of $GdBO_3$ (H-$GdBO_3$) which is not reported so far. Additional experiments were carried out to know the stability of H-forms of $EuBO_3$ and $GdBO_3$. The samples were prepared again at 900 °C using the same reactants. It was noticed that the powder XRD patterns of the products prepared at 900 °C were consistent with pure vaterite form of $EuBO_3$ and $GdBO_3$ as shown in Fig. 5(b) and (d) respectively.

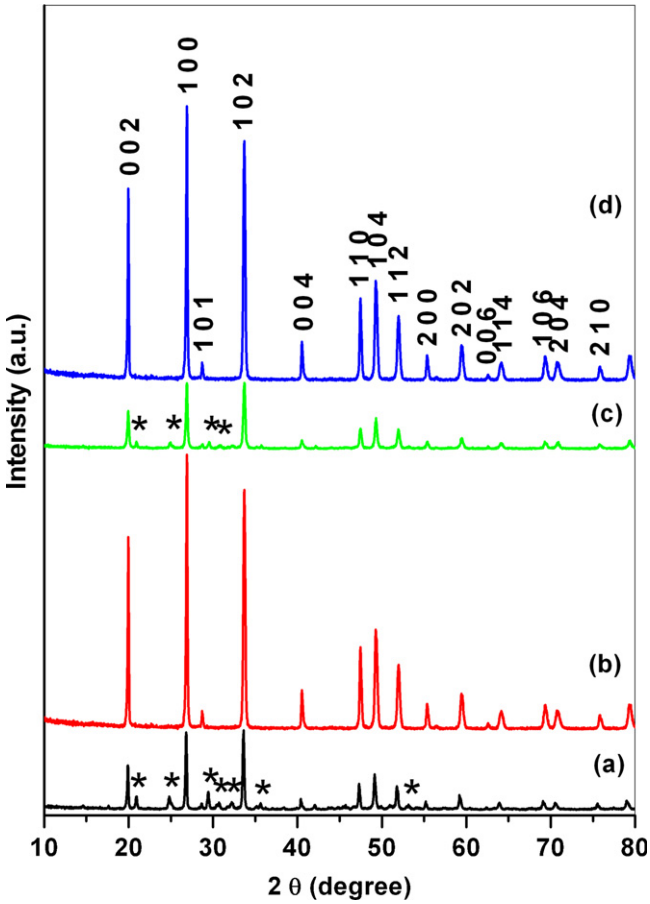

Fig. 5. Powder XRD patterns of (a) $EuBO_3$ prepared at 650 °C and (b) 900 °C, (c) $GdBO_3$ prepared at 650 °C and (d) 900 °C.

The powder XRD patterns of $DyBO_3$ and YBO_3 prepared at 650 °C contain only peaks belonging to vaterite $LnBO_3$ (Ln = Dy and Y) structure and are in good agreement with their respective JCPDS data [JCPDS Nos. 74-1933 for $DyBO_3$ and 74-1929 for YBO_3].

3.2. FT-IR spectra

Generally crystalline transition metal and rare earth borates are characterized by complex anions that arise from either planar BO_3 or tetrahedral BO_4 or both BO_3 and BO_4 units. For an isolated planar trigonal BO_3 group, six fundamental modes of vibrations are expected [25]. They are ν_1 (symmetric stretch, non degenerate, 950 cm^{-1}), ν_2 (out of plane bending, non degenerate, 740 cm^{-1}), ν_3 (antisymmetric stretch, doubly degenerate, 1250 cm^{-1}) and ν_4 (in plane bending, doubly degenerate, 600 cm^{-1}). Tetrahedral BO_4 group, on the other hand, gives nine fundamental modes of vibrations: ν_1 (symmetric stretch, non degenerate, 1000 cm^{-1}), ν_2 (bond bending, doubly degenerate, below 950 cm^{-1}), ν_3 (stretching mode, triply degenerate, near 600 cm^{-1}) and ν_4 (bending mode, triply degenerate, below 600 cm^{-1}). Rare earth orthoborates of aragonite structure and the high temperature orthoborates (H-$LnBO_3$; Ln = La, Nd, Sm and Eu) consists of planar BO_3 units whereas orthoborates having vaterite structure are characterized by BO_4 tetrahedral units [15]. FT-IR spectra of all the samples were recorded in the range 2000–400 cm^{-1}. The band positions of $TbBO_3$ were characterized by bands due to BO_4 tetrahedra (vaterite structure). Table 2 shows the FT-IR band positions of $LaBO_3$:Gd, Tb, Eu. The observed band positions are similar to its parent compound $LaBO_3$ and characteristic of planar BO_3 units [15]. The FT-IR spectrum of $PrBO_3$ is found to be similar to $LaBO_3$ and reported earlier [26]. It shows the characteristic bands due to planar BO_3 units. The FT-IR spectrum of $NdBO_3$ prepared at 650 °C shows characteristic bands due to both aragonite (planar BO_3) and its H-form (planar BO_3) [15]. On the other hand, the FT-IR spectrum of the $NdBO_3$ prepared at 900 °C is characterized by bands due to only aragonite structure (planar BO_3). Fig. 6 shows the FT-IR spectra of $SmBO_3$ prepared at 650 and 900 °C. The IR spectrum of $SmBO_3$ prepared at 650 °C (Fig. 7(a)) consists of bands belonging to H-form (BO_3 units) and vaterite structure (BO_4 tetrahedra) (shown by arrows) while the FT-IR spectrum of $SmBO_3$ prepared at 900 °C (Fig. 7(b)) is characterized by bands due to H-form (BO_3 planar) only. The FT-IR spectra of $EuBO_3$ and $GdBO_3$ prepared at 650 °C show the characteristic bands due to vaterite structure (BO_4 tetrahedra) and their H-forms (BO_3 planar) whereas the FT-IR spectra of both the samples prepared at 900 °C show only bands due to vaterite structure (BO_4 tetrahedra). These infrared spectral results are consistent with their corresponding powder XRD data [15]. The FT-IR spectra of $DyBO_3$ and YBO_3 prepared at 650 °C show

Table 2
Infrared band positions (cm^{-1}) of $LaBO_3$:Gd, Tb and Eu prepared at 650 °C/14 h.

Compound	ν_3	ν_1	ν_2	ν_4
$LaBO_3$	1280	941	789, 717	613, 594
$LaBO_3$:Gd (2.5 mol%)	1275	939	790, 713	611, 610
$LaBO_3$:Gd (5 mol%)	1273	940	791, 714	610, 592
$LaBO_3$:Gd (7.5 mol%)	1278	940	792, 713	611, 592
$LaBO_3$:Gd (10 mol%)	1279	941	791, 713	611, 592
$LaBO_3$:Tb (2.5 mol%)	1277	939	791, 713	610, 592
$LaBO_3$:Tb (5 mol%)	1274	940	792, 714	611, 592
$LaBO_3$:Tb (7.5 mol%)	1280	940	792, 713	611, 592
$LaBO_3$:Tb (10 mol%)	1281	940	792, 711	611, 592
$LaBO_3$:Eu (2.5 mol%)	1275	940	791, 714	610, 592
$LaBO_3$:Eu (5 mol%)	1275	940	791, 714	610, 592
$LaBO_3$:Eu (7.5 mol%)	1279	940	792, 707	611, 592
$LaBO_3$:Eu (10 mol%)	1282	941	791, 710	612, 592

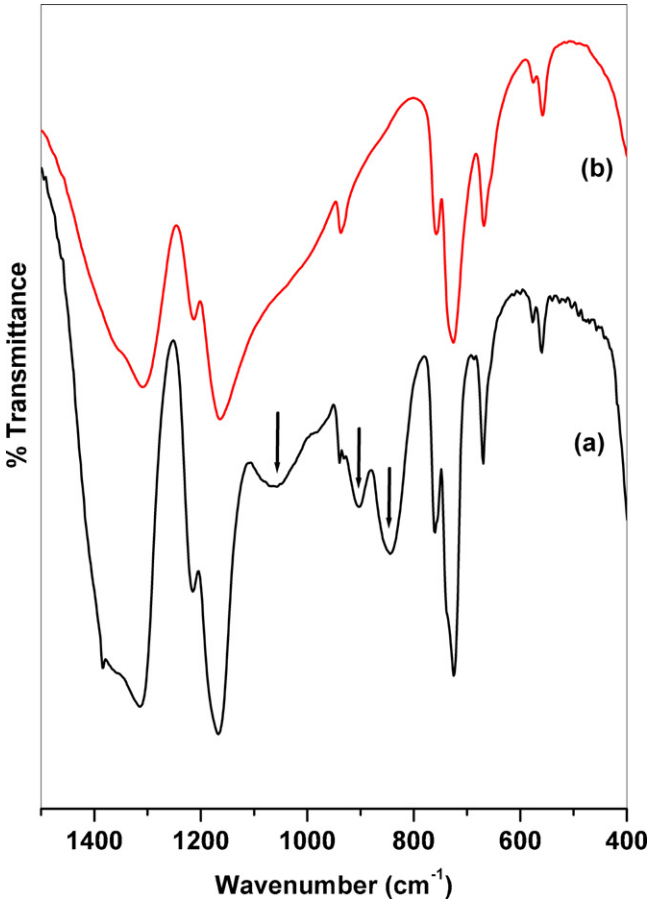

Fig. 6. FT-IR spectra of $SmBO_3$ prepared at (a) 650 °C and (b) 900 °C.

only bands due to tetrahedral BO_4 units (vaterite structure) and are consistent with powder XRD results. The band positions of all the samples prepared at 650 °C are given in Table 3 along with their assignments.

3.3. SEM

The morphology of rare earth orthoborates ($LaBO_3$, $NdBO_3$, $SmBO_3$, $EuBO_3$ and $GdBO_3$) prepared at 900 °C was examined by SEM measurements. The SEM images of representative samples are shown in Fig. 7. All the samples exhibit a distribution of particle size over a wide range. The shape of the particles is irregular.

3.4. ESR spectra of $LaBO_3$:Gd

The electronic configuration of Gd^{3+} is [Xe] $4f^7$ and its ground state is $^8S_{7/2}$. The Hamiltonian for such an ion is given by [27]

$$H = H_{Zeeman} + H_{CF} \tag{3}$$

where, H_{Zeeman} and H_{CF} correspond to Zeeman and crystal field interactions. Generally, the crystal field interactions are smaller than the Zeeman interactions. Then the Hamiltonian is composed of only Zeeman term resulting a single resonance at $g = 2$. But strong spin–orbit coupling of 4f electrons of Gd^{3+} breaks the L–S scheme of energy levels and the ground state multiplet is mixed with $L \neq 0$ states giving rise to a crystal field which is comparable to exchange coupling energy. Under these conditions the ESR spectrum is characterized by several lines. The Spin-Hamiltonian is given [28]

$$H = g\mu_B \vec{H} \cdot \vec{S} + \frac{1}{3}[b_2^0 O_2^0 + b_2^2 O_2^2] + \frac{1}{60}[b_4^0 O_4^0 + b_4^2 O_4^2 + b_4^4 O_4^4] + \frac{1}{1260}[b_6^0 O_6^0 + b_6^2 O_6^2 + b_6^4 O_6^4 + b_6^6 O_6^6] \tag{4}$$

where $\vec{H}$ is the magnetic field; $S = 7/2$; μ_B is the Bohr magneton; b_n^m are Spin-Hamiltonian parameters and O_n^m are Steven's operator equivalents [28].

The room temperature X-band powder ESR spectra of $LaBO_3$:Gd (2.5, 5, 7.5 and 10 mol%) is shown in Fig. 8. These spectra are characterized by several anisotropic lines and are similar to those reported for Gd:$LnPO_4$, Gd:$ZrSiO_4$, Gd:$InBO_3$ and Gd:$Y_2Ti_2O_7$ [28–30]. It is observed that the intensity of the ESR signal decreases with increasing concentration of Gd^{3+} from 2.5 to 10 mol%. At 2.5 mol% of Gd^{3+}, the ESR lines were sharp compared to the other concentrations due to the less number of Gd^{3+} ions on the surface. As the Gd^{3+} ion concentration increases, the number of Gd^{3+} ions on the surface increases resulting in the broadening of the lines. Therefore, 2.5 mol% is considered as optimum concentration above which the spin–spin interactions of Gd^{3+} become dominant. The Spin-Hamiltonian parameters were obtained for this concentration from its ESR data using expressions reported [28] and are given in Table 4.

Brodbeck and Iton have classified the different types of powder ESR of Gd^{3+} based on the magnitude of $H_{CF}/h\nu$, where H_{CF} is crystal field interactions [31]. Based on the ratio of $H_{CF}/h\nu$, the ESR spectra are divided into three categories: (a) weak, (b) intermediate and (c) strong.

Table 3
Infrared band positions (cm^{-1}) of $LnBO_3$ (Ln = Pr, Nd, Sm, Eu, Gd, Tb, Dy and Y) prepared at 650 °C/14 h.

$PrBO_3$	$NdBO_3$	$SmBO_3$	$EuBO_3$	$GdBO_3$	$TbBO_3$	$DyBO_3$	YBO_3
	1382ν_3 (H-form)	1384ν_3 (H-form)		1384ν_3 (H-form)			
1282ν_3 (aragonite)	1294ν_3 (H-form)	1315ν_3 (H-form)	1312ν_3 (H-form)	1325ν_3 (H-form)			
	1213ν_3 (H-form)	1215ν_3 (H-form)	1216ν_3 (H-form)	1217ν_3 (H-form)			
	1165ν_3 (H-form)	1166ν_3 (H-form)	1162ν_3 (H-form)	1170ν_3 (H-form)			
	1050ν_3 (aragonite)	1058 (vaterite)		1072 (vaterite)	1074 (vaterite)	1078 (vaterite)	1085 (vaterite)
			1023 (vaterite)		1018 (vaterite)	1013 (vaterite)	1011 (vaterite)
947ν_1 (aragonite)	950ν_1 (aragonite)	939ν_1 (H-form)					
		902 (vaterite)	911 (vaterite)	910 (vaterite)	916 (vaterite)	917 (vaterite)	912 (vaterite)
		844 (vaterite)	860 (vaterite)	858 (vaterite)	860 (vaterite)	856 (vaterite)	860 (vaterite)
791ν_2 (aragonite)	790ν_2 (aragonite)						
	760ν_2 (H-form)	759ν_2 (H-form)	758ν_2 (H-form)	761ν_2 (H-form)			
715ν_2 (aragonite)	723ν_2 (H-form)	725ν_2 (H-form)	724ν_2 (H-form)	725ν_2 (H-form)			
			690 (vaterite)	696 (vaterite)	700 (vaterite)	702 (vaterite)	711 (vaterite)
	665ν_4 (H-form)	669ν_4 (H-form)	669ν_4 (H-form)	677ν_4 (H-form)			
615ν_4 (aragonite)	619ν_4 (aragonite)						
594ν_4 (aragonite)	596ν_4 (aragonite)	576ν_4 (H-form)	573ν_4 (H-form)				
	559ν_4 (H-form)	559ν_4 (H-form)	557 (vaterite)	563 (vaterite)	567 (vaterite)	568 (vaterite)	570 (vaterite)

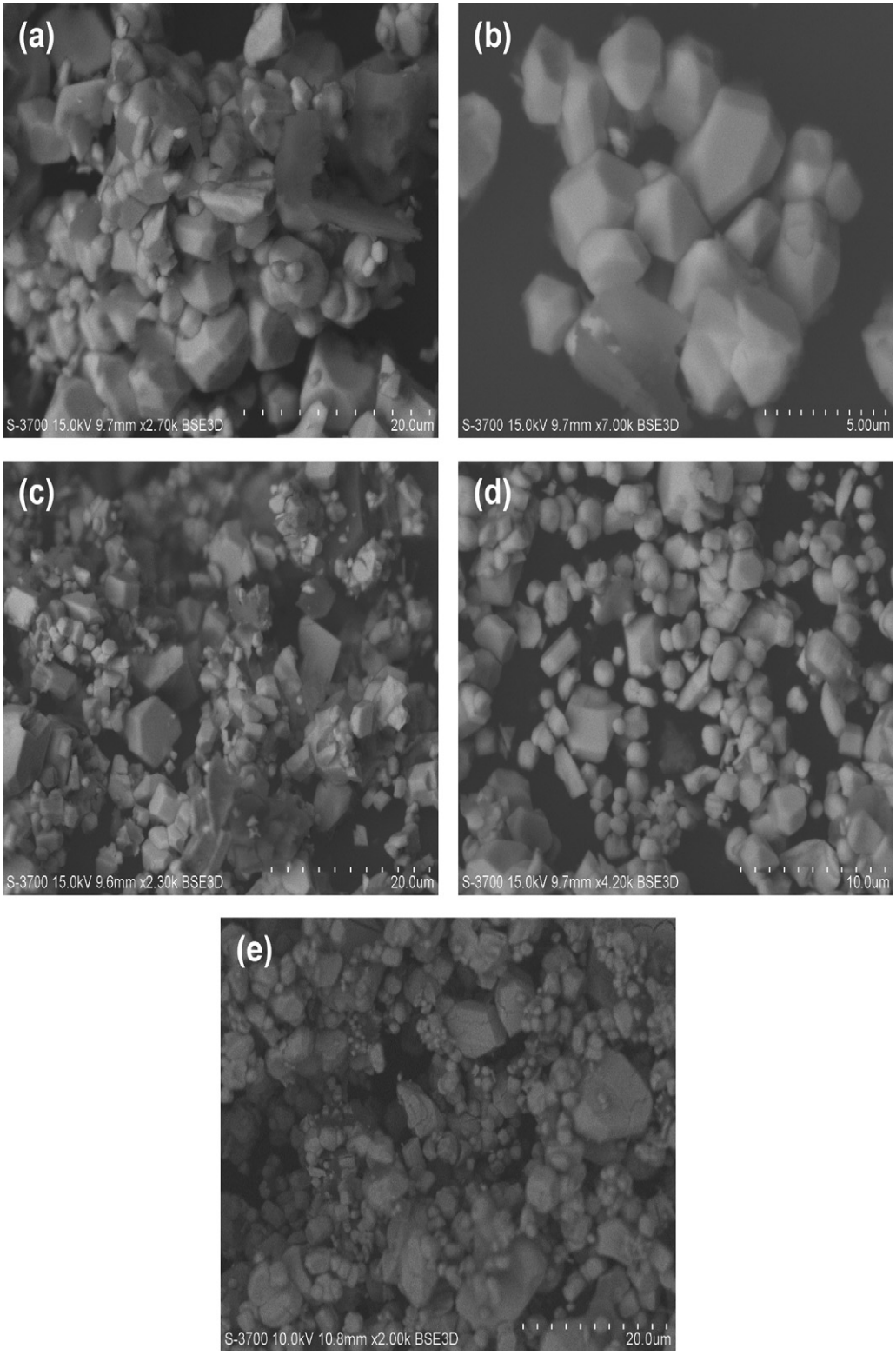

Fig. 7. SEM images of (a) $LaBO_3$, (b) $NdBO_3$, (c) $SmBO_3$, (d) $EuBO_3$ and (e) $GdBO_3$ prepared at 900 °C.

(a) *Weak*: In this category, $H_{CF}/h\nu \leq 1/4$ and higher order transitions with $g > 2.0$ are strongly forbidden due to the weak H_{CF}. Thus, the spectra are primarily concentrated in the vicinity of $g \sim 2.0$.

(b) *Intermediate*: It is characterized by $1/4 \leq H_{CF}/h\nu \leq 4$. This category is further divided in to two parts: (i) lower CF strength region $1/4 < H_{CF}/h\nu < 1$ and (ii) higher CF strength region $1 < H_{CF}/h\nu < 4$. In the lower intermediate category, the ESR spectra consist of a wide dispersion of resonances with g values in the range $2.0 < g < \infty$. In the higher CF strength region, the ESR spectrum consists of a group of resonances with $g > 2.0$.

(c) *Strong*: In this category $H_{CF}/h\nu \geq 4$, the ESR spectrum is entirely controlled by the few resonances resulting from transitions within the Kramer's levels.

In the present investigation, the ESR spectrum of $LaBO_3$:Gd (2.5 mol%) is characterized by several lines with $g > 2.0$. The value

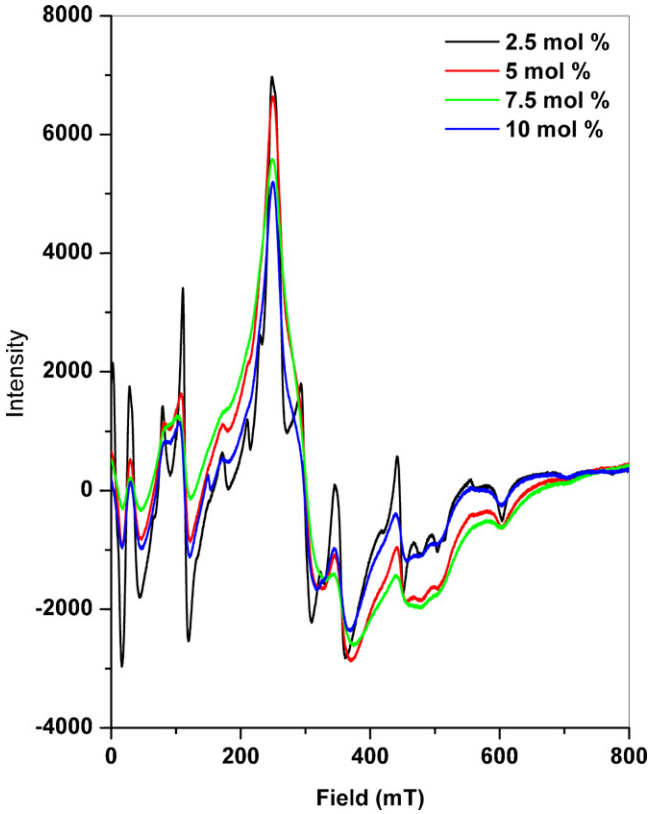

Fig. 8. ESR spectra of $LaBO_3$:Gd (2.5, 5, 7.5 and 10 mol%).

of $H_{CF}/h\nu$ is found to be 1.1. Therefore, it belongs to the intermediate category on the higher side of the CF strength i.e. $1 < H_{CF}/h\nu < 4$.

3.5. Luminescence spectra

$LaBO_3$ crystallizes in aragonite structure with C_s point group symmetry and La^{3+} ions are in ninefold coordination to oxide ligands [32]. On the other hand, $GdBO_3$ or $TbBO_3$ or $EuBO_3$ crystallizes in vaterite type structure with D_{3d} point group symmetry and Gd^{3+} or Tb^{3+} or Eu^{3+} ions are coordinated to eight oxygen ions [33]. However, when a small quantity of Gd^{3+} or Tb^{3+} or Eu^{3+} ($\leq$ 10 mol%) is doped into $LaBO_3$, its aragonite structure remains unchanged as shown by their powder XRD data. Thus, Gd^{3+}, Tb^{3+} and Eu^{3+} ions are expected to occupy the La^{3+} position and its local environment is not altered. The luminescence studies of $LaBO_3$:Tb, Eu are given below.

3.5.1. $LaBO_3$:Tb

Fig. 9a (inset) shows the excitation spectra of $LaBO_3$:Tb (2.5, 5, 7.5 and 10 mol%) under the emission wavelength of 543 nm. These spectra are characterized by peaks due to $^7F_6 \rightarrow {}^5H_6$ (304 nm), $^7F_6 \rightarrow {}^5D_0$ (318 nm), $^7F_6 \rightarrow {}^5D_2$ (352 nm), $^7F_6 \rightarrow {}^5L_{10}$ (359 nm), $^7F_6 \rightarrow {}^5G_6$ (371 nm), $^7F_6 \rightarrow {}^5D_3$ (378 nm) and $^7F_6 \rightarrow {}^5D_4$ (487 nm)

Table 4
Spin-Hamiltonian parameters (in $10^{-4}\,cm^{-1}$) of $LaBO_3$:Gd.

	$LaBO_3$:Gd (2.5 mol%)
g	2.06753 ± 0.001
b_2^0	561.05 ± 5.0
b_4^0	2.97 ± 5.0
b_6^0	-7.82 ± 5.0
b_2^2	370.53 ± 5.0
b_4^4	-5.17 ± 5.0

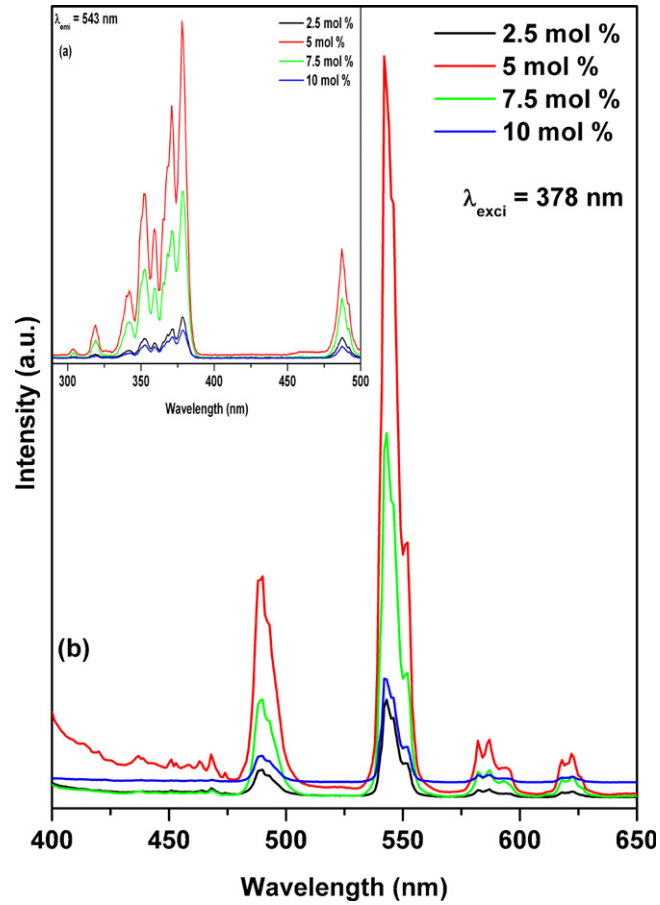

Fig. 9. (a) (inset) Excitation and (b) emission spectra of $LaBO_3$:Tb (2.5, 5, 7.5 and 10 mol%).

transitions. Since the absorption at 378 nm is maximum, it is fixed as excitation wavelength for recording the emission spectra. The emission spectra of $LaBO_3$:Tb (2.5, 5, 7.5 and 10 mol%) is shown in Fig. 9b. The intensity of all the transitions follows the order: 5 > 7.5 > 10 > 2.5 mol%. The emission intensity increases up to 5 mol% and then decreases. Thus the critical concentration above which the concentration quenching (arising due to cross-relaxation between neighboring Tb^{3+} ions) becomes dominant was found to be 5 mol%. The non-linear variation in the emission intensity with the increase in the concentration of Tb^{3+} ions indicates the formation of doped compounds ($LaBO_3$:Gd) and not the mixture ($1 - x LaBO_3$ and $x TbBO_3$). The emission intensity is expected to increase steadily with increase in the rare earth ion (Tb^{3+}) concentration, if the compounds form the mixture [34]. The emission spectrum of $LaBO_3$:Tb (5 mol%) is characterized by f–f transitions: $^5D_4 \rightarrow {}^7F_6$ (480–500 nm), $^5D_4 \rightarrow {}^7F_5$ (535–560 nm), $^5D_4 \rightarrow {}^7F_4$ (578–598 nm) and $^5D_4 \rightarrow {}^7F_3$ (614–627 nm). It is similar to those reported for $LuBO_3$:Tb, $GdBO_3$:Tb and YBO_3:Tb [35–37].

3.5.2. $LaBO_3$:Eu

The excitation and emission spectra of $LaBO_3$:Eu (2.5, 5, 7.5 and 10 mol%) are similar to those reported earlier [38–40]. The intensity of all the transitions follows the order: 5 > 7.5 > 10 > 2.5 mol%. Hence, 5 mol% was found to be critical concentration for Eu^{3+} doped in $LaBO_3$ also.

3.6. Physical properties

All the rare earth borates prepared by solid state method are characterized by powder XRD and IR spectroscopy. The powder

XRDs and IR spectra of these borates are similar to those prepared by metathesis reaction and reported earlier [10]. Physical properties of the borates prepared by metathesis and conventional solid state method are compared. The physical properties such as density and room temperature AC conductivity are measured for representative borate $LaBO_3$ synthesized by metathesis and solid state routes. The experimental and theoretical (from X-ray diffraction) densities of $LaBO_3$ obtained by metathesis are 4.93 and 5.28 g/cm^3 and those obtained by solid state route are 5.17 and 5.37 g/cm^3 respectively. The percentage of experimental and theoretical densities is 96% in solid state sintering route and 93% in metathesis reaction method. The reported density of $LaBO_3$ is 5.309 g/cm^3 [10]. The density values obtained in the present investigations are close to the value reported. The AC conductivity at 1 MHz frequency for $LaBO_3$ synthesized by metathesis reaction is 1.5×10^{-3} (ohm m)$^{-1}$ and that synthesized by solid state route is 1.0×10^{-3} (ohm m)$^{-1}$. These values match well within the experimental error.

4. Conclusions

Rare earth orthoborates, $LnBO_3$ (Tb, La, Pr, Nd, Sm, Eu, Gd, Dy, Y) and $LaBO_3$:Gd, Tb, Eu have been synthesized by metathesis reaction between sodium meta borate and $LnCl_3$. They were characterized by powder XRD and FT-IR spectroscopy. $TbBO_3$ (vaterite), $LaBO_3$, $LaBO_3$:Gd, Tb, Eu (aragonite), $PrBO_3$ (aragonite), $DyBO_3$ (vaterite) and YBO_3 (vaterite) crystallized in pure phases at 650 °C/14 h. On the other hand, $NdBO_3$ (aragonite + H-form), $EuBO_3$ (vaterite + H-form) and $GdBO_3$ (vaterite + H-form) crystallized in mixed phases at 650 °C/14 h with H-form as minor phase. In the case of $SmBO_3$, the H-form was found to be major phase at 650 °C/14 h. At higher temperatures (900 °C/6 h), minor phases were disappeared and pure phases were obtained for these borates. Infrared spectral results show that aragonite structure and H-forms have trigonal planar BO_3 groups, while vaterite structure has BO_4 tetrahedral groups. These results are consistent with powder XRD results. The SEM images of these rare earth borates show irregular shape with wide distribution of crystallites. ESR spectra of $LaBO_3$:Gd was characterized by several anisotropic lines with $g > 2.0$. The Spin-Hamiltonian parameters were calculated and belong to higher side of the "intermediate category". The luminescence spectra of $LaBO_3$:Tb, Eu gave characteristic Tb^{3+} or Eu^{3+} bands.

Acknowledgements

The authors thank Department of Science and Technology (DST No. SR/S1/PC-04/2007), New Delhi for providing financial assistance.

References

[1] A.J. Kurtzig, R. Wolfe, R.C. LeCraw, J.W. Nielsen, Appl. Phys. Lett. 14 (1969) 350–352.
[2] R.C. LeCraw, presented orally at INTERMAG, Stuttgard, Germany, 1966 (unpublished);
J.F. Dillon Jr., J. Appl. Phys. 39 (1968) 922.
[3] T.A. Bither, C.G. Frederick, T.E. Gier, J.F. Weiher, H.S. Young, Solid State Commun. 8 (1970) 109–112.
[4] Z.G. Wei, L.D. Sun, C.S. Liao, X.C. Jiang, C.H. Yan, J. Mater. Chem. 12 (2002) 3665–3670.
[5] D.A. Keszler, Curr. Opin. Solid State Mater. Sci. 4 (1999) 155–162.
[6] D. Boyer, G. Bertrand-Chadeyron, R. Mahiou, C. Caperaa, J.C. Cousseins, J. Mater. Chem. 9 (1999) 211–214.
[7] G. Bertrand-Chadeyron, M. El-Ghozzi, D. Boyer, R. Mahiou, J.C. Cousseins, J. Alloys Compd. 317–318 (2001) 183–185.
[8] K.N. Kim, H.K. Jung, H.D. Park, J. Mater. Res. 17 (2002) 907–910.
[9] Z.H. Li, J.H. Zeng, C. Chen, Y.D. Li, J. Cryst. Growth 286 (2006) 487–493.
[10] E.M. Levin, R.S. Roth, J.B. Martin, Am. Mineral. 46 (1961) 1030–1055.
[11] J.P.R.D. Villiers, Am. Mineral. 56 (1971) 758–767.
[12] G. Chadeyron, M. El-Ghozzi, R. Mahiou, A. Arbus, J.C. Cousseins, J. Solid State Chem. 128 (1997) 261–266.
[13] J.R. Cox, D.A. Keszler, Acta Crystallogr., Sect. C 50 (1994) 1857–1859.
[14] G. Chadeyron, R. Mahiou, A. Arbus, J.C. Cousseins, VIth Eur. Conf. Solid State Chem., Zurich, September, 1997.
[15] S. Lemanceau, G. Bertrand-Chadeyron, R. Mahiou, M. El-Ghozzi, J.C. Cousseins, P. Conflant, R.N. Vannier, J. Solid State Chem. 148 (1999) 229–235.
[16] T. Takada, H. Yamamoto, K. Kageyama, Jpn. J. Appl. Phys. 42 (2003) 6162–6167.
[17] J. Ma, Q. Wu, J. Am. Ceram. Soc. 90 (2007) 3890–3895.
[18] S. Hosokawa, Y. Tanaka, S. Iwamoto, M. Inoue, J. Mater. Sci. 43 (2008) 2276–2285.
[19] Y.J. Seo, D.J. Shin, Y.S. Cho, J. Am. Ceram. Soc. 89 (2006) 2352–2355.
[20] A. Nakatsuka, O. Ohtaka, H. Arima, N. Nakayama, T. Mizota, Acta Cryst. E62 (2006) i103–i105.
[21] J. Lin, Y. Huang, J. Zhang, X. Ding, S. Qi, C. Tang, Mater. Lett. 61 (2007) 1596–1600.
[22] E. Wu, J. Appl. Crystallogr. 22 (1989) 506–510.
[23] I.V. Tananaev, Inorg. Mater. 2 (1966) 10.
[24] Y. Laureiro, M.L. Veiga, F. Fernandez, R. Saez Puche, A. Jerez, C. Pico, J. Less-Common Met. 167 (1991) 387–393.
[25] C.E. Weir, E.R. Lippincott, J. Res. NBS 65A (1961) 173.
[26] J.P. Laperches, P. Tarte, Spectrochim. Acta 22 (1966) 1201–1210.
[27] A. Abragam, B. Bleaney, Electron Paramagnetic Resonance of Transition Metal Ions, Oxford University Press, London, 1970.
[28] M. Rappaz, M.M. Abraham, J.O. Ramey, L.A. Boatner, Phys. Rev. B 23 (1981) 1012–1030.
[29] R. Velchuri, B.V. Kumar, V.R. Devi, K.R. Kumar, G. Prasad, M. Vithal, Spectrochim. Acta A 74 (2009) 726–730.
[30] B.V. Kumar, R. Velchuri, V.R. Devi, G. Prasad, B. Sreedhar, C. Bansal, M. Vithal, J. Appl. Phys. 108 (2010) 044906.
[31] C.M. Brodbeck, L.E. Iton, J. Chem. Phys. 83 (1985) 4285–4299.
[32] E. Antic-Fidancev, M. Lemaitre-Blaise, J. Chaminade, P. Porcher, J. Alloys Compd. 180 (1992) 223–228.
[33] W.F. Bradley, D.L. Graf, R.S. Roth, Acta Crystallogr. 21 (1966) 283–287.
[34] M.L. Pang, J. Lin, J. Fu, R.B. Xing, C.X. Luo, Y.C. Han, Opt. Mater. 23 (2003) 547–558.
[35] Y.H. Wang, C.F. Wu, J.C. Zhang, Mater. Res. Bull. 41 (2006) 1571–1577.
[36] J. Yang, C. Zhang, L. Wang, Z. Hou, S. Huang, H. Lian, J. Lin, J. Solid State Chem. 181 (2008) 2672–2680.
[37] G. Jia, H. You, M. Yang, L. Zhang, H. Zhang, J. Phys. Chem. C 113 (2009) 16638–16644.
[38] E.P. Riedel, J. Lumin. 1,2 (1970) 176–190.
[39] V. Jubera, J.P. Chaminade, A. Garcia, F. Guillen, C. Fouassier, J. Lumin. 101 (2003) 1–10.
[40] M. Tukia, J. Holsa, M. Lastusaari, J. Niittykoski, Opt. Mater. 27 (2005) 1516–1522.